Tunnelling and Underground Space Technology 144 (2024) 105563

Contents lists available at ScienceDirect

Tunnelling and Underground Space Technology incorporating Trenchless Technology Research

journal homepage: www.elsevier.com/locate/tust

Assessing and exploiting the interaction between ventilation and geothermal systems in an underground data centre

Sofie ten Bosch [a,*], Elena Ravera [a], Marco Tobler [b], Marco Bettelini [b], Lyesse Laloui [a]

[a] Swiss Federal Institute of Technology in Lausanne, EPFL, Laboratory of Soil Mechanics, Lausanne, Switzerland
[b] Amberg Engineering Ltd, Regensdorf-Watt, Switzerland

ARTICLE INFO

Keywords:
Underground data centre
Energy geostructures
Ventilation system
Numerical modelling
Computational fluid dynamics

ABSTRACT

Digitalization and population growth lead to the development of underground data centres, while simultaneously current climate goals stimulate the development of renewable energy sources. In this framework, this study evaluates the so far unexplored domain of geothermal activation of an underground data centre using numerical modelling. Computational fluid dynamics simulations are used to properly represent the air domain. The focus of the work lies on the analysis of the interaction between ventilation and geothermal systems in the data centre, a topic that has never been evaluated for energy geostructures in general. This leads to the possibility of suboptimal air ventilation system design and thus a potential for optimization, especially in underground data centres where daily ventilation requirements are determined by air temperature limitations. The analysis first explores the sensitivity of geothermal potential to varying ventilation conditions (airflow velocities), heat release conditions in the data centre and fluid velocities in the pipes of the geothermal activation. The impact of geothermal activation on air temperature in the underground data centre cavern is then assessed and thus the consequent impact on the ventilation system. Geothermal activation of a section of the cavern leads to a regional decrease in air temperature, which allows optimization of the whole system by reducing mechanical ventilation requirements while still respecting the temperature limitations within the data centre. The economic and environmental benefits of this optimization are also explored. Overall, it is proven that ventilation conditions have an influence on the geothermal potential that can be extracted, and optimization of the complete system is possible when considering the effect of geothermal heat extraction in underground data centres while determining their ventilation requirements.

1. Introduction

The need for clean energy sources is increasing due to current climate goals and population growth. One type of energy source that has received significant interest is the use of shallow geothermal energy, where shallow systems take advantage of the heat of the Earth's crust. In the past three decades, a new technology in this family has emerged: energy geostructures. These are structures where shallow geothermal heat exchangers are integrated in structural elements that are in contact with the ground (Laloui & Rotta Loria, 2019).

At the same time, the trend of digitalization in the 21st century caused a sharp increase in the use of data centres. It is estimated that data centres use approximately 1 % of global electricity (IEA, 2017) and this percentage is only expected to grow in the future, following current trends in society. This increasing interest causes a demand for space where data centres can be constructed. The use of underground space is becoming increasingly popular to help provide for this space in a society with an increasing world population and dense urban environments. A more complicated aspect of the development of these structures is that underground climate change through rising ground temperature surrounding the data centre from heat generated through the thermal dissipation of IT components has to be considered. Moreover, it is known that the energy consumption for cooling purposes of data centres can take up to 30 to 50 % of its total energy consumption (Zhang et al., 2014). It is therefore important to evaluate what role geothermal activation of underground data centres, a field that remains currently unexplored, can play in these aspects.

Numerical evaluations of geothermally activated underground infrastructure often use a simplified way of accounting for the air domain in the energy infrastructure (e.g., Dornberger et al., 2022).

* Corresponding author.
E-mail address: sofie.tenbosch@epfl.ch (S. ten Bosch).

https://doi.org/10.1016/j.tust.2023.105563
Received 7 June 2023; Received in revised form 8 November 2023; Accepted 14 December 2023
Available online 23 December 2023

Instead of including a full model of the airflow, the impact of the air domain is usually approximated through a boundary condition consisting of a representative air temperature and a heat transfer coefficient. This makes it impossible to assess the influence of geothermal activation of this infrastructure on the temperature of the air domain, which is an essential factor for underground data centres. Only few studies consider the full air domain for energy tunnels (Bidarmaghz et al., 2021; Bidarmaghz & Narsilio, 2018; Makasis et al., 2020; Peltier et al., 2019; Wojnarowicz, 2020) but never has the focus been on cooling of underground data centres. Additionally, the unexplored domain of the interaction between geothermal and ventilation systems in general leads to the possibility of suboptimal ventilation design for geothermally activated underground infrastructure (Bidarmaghz & Narsilio, 2018) and thus leaves a potential for optimization of both systems.

This study numerically investigates geothermal activation of a nine-cavern underground data centre located deep within a rock domain. The work focuses on the interaction between geothermal and ventilation systems to enhance the already proven benefits of these energy geostructures as renewable energy providers. Ventilation requirements in such centres are often determined by air temperature limitations, highlighting optimization potential. The study looks into the ground heat exchangers' ability to recover thermal energy, which would otherwise be expelled through mechanical ventilation, and how geothermal activation influences ventilation needs. The study first presents the modelling framework, followed by results on geothermal potential and ventilation system optimization. Economic and environmental impact of these findings are assessed for a specific scenario and the overall conclusions are presented.

2. Methodology and mathematical formulation

2.1. General

The numerical investigation examines the interaction between geothermal activation and ventilation systems in an underground data centre. The data centre in question is planned as a network of caverns for data storage containers, but not constructed yet. The scope of this study is limited to one of these caverns, using representative ground conditions, ground temperature and geometry.

Simulations are performed using COMSOL Multiphysics 6.0 (COMSOL, 2021b). 3D time-dependent analyses including computational fluid dynamics (CFD) simulations of the air domain are used to allow assessment of interactions between the air domain, the structural elements, and the rock domain surrounding the data centre.

2.2. Governing equations

To include CFD analyses for the air domain the k-ω turbulence model is selected. This model is an often-used methodology to simulate airflow at high Reynolds numbers due to its accuracy and robustness, especially for its accuracy in the prediction of the development of boundary layers and the near-wall conditions (COMSOL, 2021a; Wilcox, 1991). Equations included in this model are the Reynolds-Averaged Navier-Stokes (RANS) equations and the Wilcox revised two-equations k-ω model (Wilcox, 2008).

The RANS method does not address all time and space scales of the turbulent flow. Instead, it transforms the Navier-Stokes equations so that small-scale turbulent fluctuations do not need to be simulated directly, by using approximations instead. The computational effort needed to obtain all information on the fluctuations in time and space is generally excessively large and the average representation that can be obtained using the RANS equations provides sufficient information for engineering purposes. In this study, numerical analyses of the airflow in the underground data centre are performed under steady-state conditions and due to the low Mach number (Ma $<$ 0.1) the fluid is considered weakly compressible (air density is only a function of temperature and does not depend on pressure). Therefore, the equations for conservation of momentum and mass implemented in the modelling framework read:

$$\nabla\cdot(\rho_a \boldsymbol{v_a}) = 0 \tag{1}$$

$$\rho_a(\boldsymbol{v_a}\cdot\nabla)\boldsymbol{v_a} = \nabla\cdot[-p\boldsymbol{I}+\boldsymbol{K}] + (\rho_a - \rho_{ref})\boldsymbol{g} \tag{2}$$

$$\boldsymbol{K} = (\mu+\mu_T)\left(\nabla\boldsymbol{v_a} + (\nabla\boldsymbol{v_a})^T\right) - \frac{2}{3}(\mu+\mu_T)(\nabla\cdot\boldsymbol{v_a})\boldsymbol{I} - \frac{2}{3}\rho_a k\boldsymbol{I} \tag{3}$$

$$\mu_T = \rho_a\frac{\mathrm{k}}{\omega} \tag{4}$$

where ρ_a and p represent the air density and reduced pressure, $\boldsymbol{v_a}$ the airflow velocity, $\boldsymbol{g}$ the gravitational acceleration vector, I the identity matrix, ρ_{ref} the constant reference density, μ the dynamic viscosity and μ_T the turbulent viscosity (eddy viscosity). Influence of gravity is accounted for in this framework and reduced pressure condition is used. The parameters k and ω are the turbulent kinetic energy and the turbulent dissipation rate, respectively. The used k-ω model is a two-equation model that consists of two equations used to predict the evaluation of these parameters, formulated as

$$\rho_a(\boldsymbol{v_a}\cdot\nabla)k = \nabla\cdot\left[\left(\mu+\mu_T\sigma_k^*\right)\nabla k\right] + P_k - \beta^*\rho_a\omega k \tag{5}$$

$$\rho_a(\boldsymbol{v_a}\cdot\nabla)\omega = \nabla\cdot[(\mu+\mu_T\sigma_\omega)\nabla\omega] + \alpha\frac{\omega}{k}P_k - \rho_a\beta\omega^2 \tag{6}$$

with the production term being

$$P_k = \mu_T\left[\nabla\boldsymbol{v_a} : \left(\nabla\boldsymbol{v_a} + (\nabla\boldsymbol{v_a})^T\right) - \frac{2}{3}(\nabla\cdot\boldsymbol{v_a})^2\right] - \frac{2}{3}\rho_a k\nabla\cdot\boldsymbol{v_a} \tag{7}$$

and the other model parameters can be calculated by

$$\beta = \beta_0 f_\beta, \beta^* = \beta_0^* f_{\beta^*}$$

$$f_\beta = \frac{1+70\chi_\omega}{1+80\chi_\omega}, \chi_\omega = \left|\frac{\Omega_{ij}\Omega_{jk}S_{ki}}{(\beta_0^*\omega)^3}\right|,$$

$$f_{\beta^*} = \begin{cases} 1, \chi_k \le 0 \\ \dfrac{1+680\chi_k^2}{1+400\chi_k^2}, \chi_k > 0 \end{cases}, \chi_k = \frac{1}{\omega^3}(\nabla k\cdot\nabla\omega) \tag{8}$$

where the mean rotation-rate tensor and the mean strain-rate tensor are respectively

$$\Omega_{ij} = \frac{1}{2}\left(\frac{\partial\overline{v}_{ai}}{\partial x_j} - \frac{\partial\overline{v}_{aj}}{\partial x_i}\right), \mathrm{S}_{ij} = \frac{1}{2}\left(\frac{\partial\overline{v}_{ai}}{\partial x_j} + \frac{\partial\overline{v}_{aj}}{\partial x_i}\right) \tag{9}$$

Values of the model constants that are used in these equations are shown in Table 1.

Some approximations for the mixing length limit and realizability constraints are implemented, given by the following equations based on concepts from Kuzmin et al. (2007)

$$\frac{\omega}{k} \approx \frac{\rho_a}{\max(\mu_T, eps)} \tag{10}$$

Table 1
Turbulence model parameters.

Constant	Value
α	13/25
$\sigma_k{}^*$	1/2
σ_ω	1/2
β_0	9/125
$\beta_0{}^*$	9/100

$$\frac{1}{\omega} \approx \frac{l_{\mathrm{mix}}^2 \rho_a}{\max(\mu_T, eps)} \tag{11}$$

in which eps is a small number (1E-16) that is used to regularize expressions where a denominator could assume a zero value during solver iterations and

$$l_{\mathrm{mix}} = \min\left(\frac{\sqrt{k}}{\omega}, l_{\mathrm{mix}}^{\mathrm{lim}}, l_r\right) \tag{12}$$

$$l_r = \frac{1}{\sqrt{6}} \frac{\sqrt{\mathrm{k}}}{\sqrt{\mathrm{S}_{ij}\mathrm{S}_{ij}}} \tag{13}$$

where $l_{\mathrm{mix}}^{\mathrm{lim}}$ is an upper limit of the mixing length, an implemented tool used to obtain better convergence.

The results from the steady-state analysis of the airflow are then used to evaluate heat transfer process in the underground data centre in a time-dependent analysis. In this way, a one-way coupling is considered which means that the heat transfer processes do not influence the airflow profile in the cavern, which for the temperature variations expected in this study does not have a significant influence on the results, however, the obtained airflow profile influences heat transfer processes in the cavern and ground domains.

For the cavern structural elements and the rock domain, conduction is assumed to be the main governing heat transfer principle. The Fourier equation is used to model this, which states the rate of heat transfer is proportional to the temperature gradient. The other main heat transfer process for the underground data centre is heat convection, which is mainly relevant for the air in the cavern where it occurs due to the natural or mechanical airflow and for the ground heat exchangers due to the fluid flow in the pipes. Heat convection as a result of a prescribed hydraulic head in the rock domain is not relevant for the analysed underground data centre. The energy conservation equation implemented in the model accounts for the variation of internal energy, both a convective and conductive term and reads:

$$\nabla\cdot(\lambda\nabla T) = \rho c_p \frac{\partial T}{\partial t} + \rho c_p \boldsymbol{v_a} \nabla T \tag{14}$$

where λ is the thermal conductivity of the related material, T the temperature and c_p the specific heat capacity.

The energy conservation equation for the incompressible fluid flowing in the pipes integrated in the cavern walls is

$$\rho_f A_p c_{p,f} \frac{\partial T_f}{\partial \mathrm{t}} + \rho_f A_p c_{p,f} \boldsymbol{v_f} \nabla T_f = \nabla\cdot A_p \left(\lambda_f \nabla T_f\right) + f_D \frac{\rho_f A_p}{2 d_h} |\boldsymbol{v_f}| \boldsymbol{v_f}^2 + \boldsymbol{q_{wall}} \tag{15}$$

where ρ_f, $c_{p,f}$, T_f, $\boldsymbol{v_f}$ and λ_f are respectively the density, the specific heat capacity, the temperature, the velocity and the thermal conductivity of the heat carrier fluid (HCF). A_p is the cross section of the pipe, f_D the Darcy friction factor and d_h the mean hydraulic diameter. The term $\boldsymbol{q_{wall}}$ represents the external heat exchange rate through the pipe wall, which is a function of the outer wall temperature and the fluid temperature as:

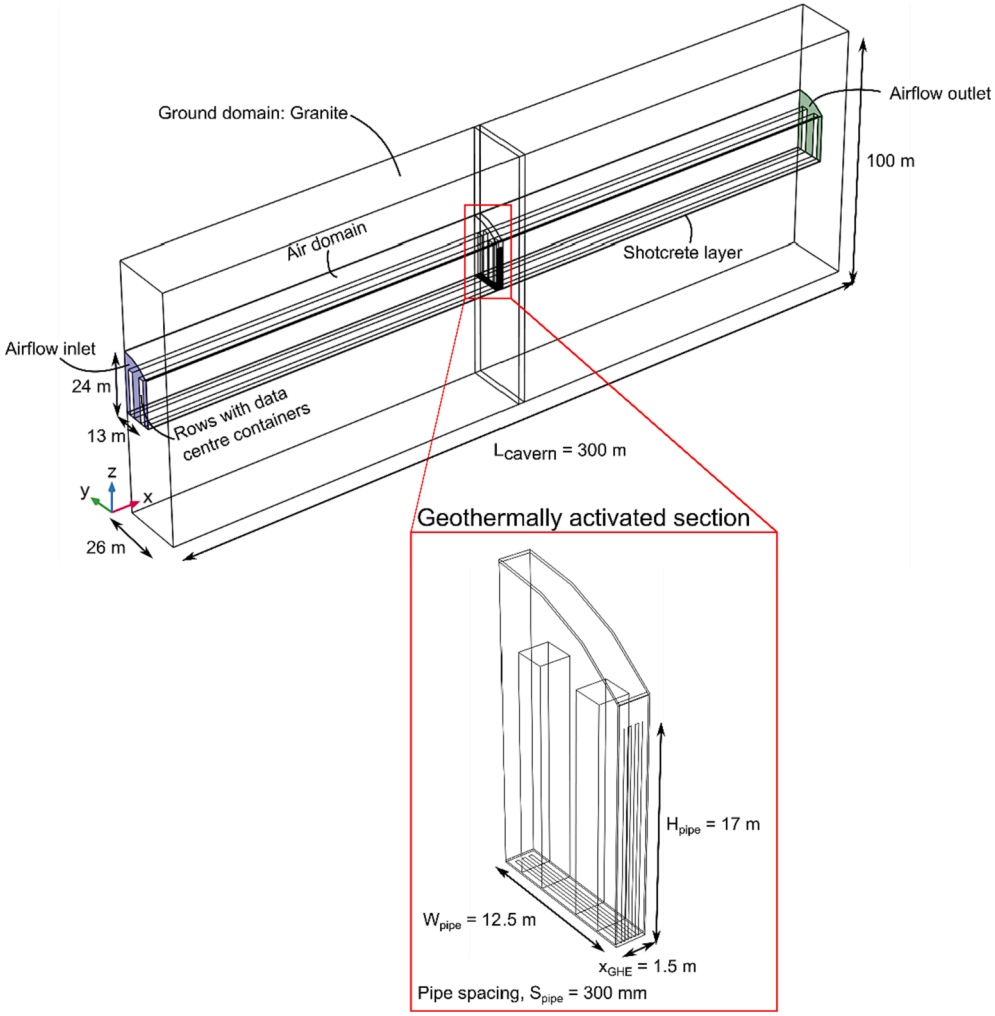

Fig. 1. Model geometry representing one cavern of the underground data centre.

$$q_{wall} = \left(hP_p\right)_{eff}\left(T_{ext} - T_f\right) \tag{16}$$

in which h is the convective heat transfer coefficient and P_p is the wall perimeter of the pipe.

2.3. Numerical model geometry

The geometry of the numerical model is presented in Fig. 1. It represents half a cavern of the data centre, which is possible using the symmetry plane along its length. The individual data centre containers are simplified to two rows along the length of the cavern with a height of 18 m and a width of 2.5 m.

The walls and slab of a cross section with a length of 1.5 m located halfway along the length of the cavern is geothermally activated, by implementing 6 geothermal pipes using a pipe spacing of 300 mm. HCF circulates in these pipes and undergoes a change in temperature, allowing to extract thermal energy. The walls and floor of the cavern are selected for geothermal activation because these are most closely located to the work domains inside the data centre where temperature limitations need to be respected. This temperature limitation is further discussed in section 3.3. The pipes are positioned one third into the shotcrete thickness, closer to the air domain than to the granite domain.

2.4. Boundary and initial conditions

Fig. 2 illustrates the boundary conditions applied to the model. A Dirichlet boundary condition is used to specify the temperature at the top and bottom boundaries of the model. The temperature is set as equal to the undisturbed ground temperature because the cavern lies sufficiently deep below the surface level not to account for the influence of surface temperature variations. Symmetry conditions are applied at both longitudinal sides of the model domain, used to represent the full cavern geometry and other caverns parallel to the presented one. At the inlet and outlet planes of the cavern, an adiabatic boundary condition with no heat flux is applied to the ground and shotcrete domains. A fixed inlet temperature boundary condition is applied on the air inflow side of the cavern, set as equal to the ground temperature. At the airflow outlet, a symmetry boundary condition is used for the thermal component, this way the cavern is considered as a section of a larger cavern. At the sides of the data centre containers a heat flux representing the heat generated by the IT equipment is imposed, q_{data}.

$$-\mathbf{n}\cdot\mathbf{q} = q_{data} \tag{17}$$

The value of the heat flux implemented is 125 W/m^2, unless specified otherwise. Considering a heat release of 50 kW per prefabricated all-in-one data container, the value of 125 W/m^2 represents a scenario with 70 % direct water cooling of the IT equipment and 30 % of the heat released into the cavern. An adiabatic, zero heat flux condition is applied, at the top and bottoms of the container rows assuming that these surfaces are thermally isolated.

Airflow boundary conditions are specified for the air domain of the cavern. A fully developed flow boundary condition with a fixed average airflow velocity, equal to 2 m/s unless specified otherwise, is applied at the inlet of the cavern. At the outlet a fully developed flow boundary condition is applied with an average pressure of 0 Pa. Wall functions for rough walls are used to simulate the flow in the near-wall regions along the cavern walls and data centre container walls. A no slip wall condition is used with a sand roughness model, using an equivalent sand roughness height of 0.3 mm to represent a concrete interface. A Neumann boundary condition is used for the turbulent kinetic energy, k, Eq. 18, and Eq. 19 gives the boundary condition for the turbulent dissipation rate

$$\mathbf{n}\cdot\nabla k = 0 \tag{18}$$

$$\omega = \frac{\rho_a k}{\kappa \delta_w^+ \mu} \tag{19}$$

where δ_w^+ is the wall resolution, which defines a theoretical lift-off of the computational domain from the wall as part of the wall functions. It is defined as

$$\delta_w^+ = \max\left\{11.06, \frac{k_s^+}{2}, \frac{h^+}{2}\right\} \tag{20}$$

with k_s^+ is the roughness height and h^+ height of the boundary mesh cell in viscous units

$$k_s^+ = \frac{\rho_a \beta_0^{*1/4} \sqrt{k}}{\mu} k_s \tag{21}$$

in which k_s is the equivalent sand roughness height (Nikuradse, 1933).

Initially all components have a temperature equal to the ground temperature. A summary of the relevant model parameters is presented

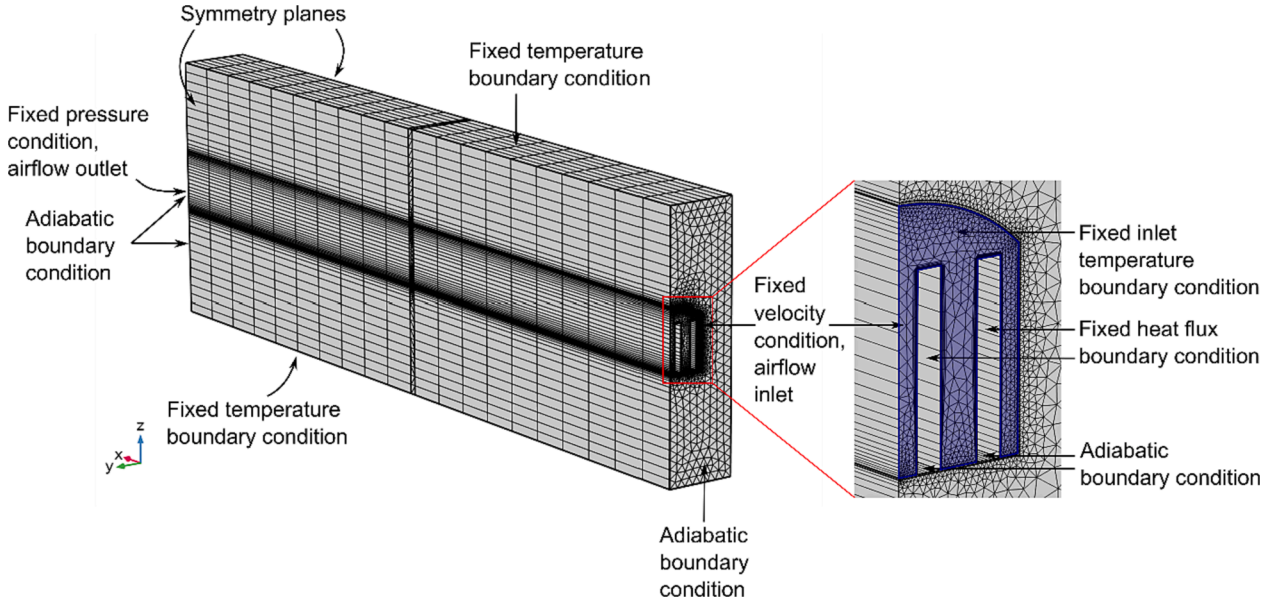

Fig. 2. Mesh and boundary conditions used for the underground data centre cavern.

in Table 2. Initially zero airflow and zero pressure conditions are used in the air domain, together with the following conditions for the turbulent kinetic energy and the specific dissipation rate:

$$k_{\text{init}} = \left(\frac{10 \cdot \mu}{\rho_a (0.1 \cdot l_{\text{mix}}^{\text{lim}})} \right)^2 \tag{22}$$

$$\omega_{\text{init}} = \frac{\sqrt{k_{\text{init}}}}{0.1 \cdot l_{\text{mix}}^{\text{lim}}} \tag{23}$$

2.5. Meshing and simulation time

The mesh used for the simulations with one geothermally activated section halfway of the cavern is shown in Fig. 2 and consists of 44,064 tetrahedral elements, 13 pyramids, 63,483 prisms, 22,545 hexahedral elements, 14,627 triangles, 13,118 quads, and 2878 edge and vertex elements. Boundary layer meshing is used on boundaries between the air domain and the shotcrete or data centre containers to better represent the thin boundary layers along these no-slip boundaries. The geothermal pipes are implemented as one-dimensional edge elements. This is a commonly used modelling strategy for energy geostructures (Rotta Loria, 2020).

Simulations for the thermal field are performed for a simulated time period of 100 days, to achieve reasonable steady state conditions. This time period is longer than typically found in other studies evaluating geothermal potential of energy infrastructures (Cousin et al., 2019; Wojnarowicz, 2020; Zannin et al., 2022), due to the effect of the heat generation component in this cavern, which is generally not accounted for or not applicable to other typically evaluated case studies. Steady conditions are assumed to be reached when the difference of the extracted thermal power is smaller than 0.5 % compared to the one of the previous day, a methodology previously applied by Cousin et al. (2019), shown as:

$$\dot{q}_i(t_{steady}) - \dot{q}_i(t_{steady} + 24 \ \ hours) \leqslant 0.5\% \cdot \dot{q}_i(t_{steady}) \tag{24}$$

calculating the geothermal potential for this check is done using

$$q = \frac{\rho_f c_{p,f} \dot{V} (T_{out} - T_{in})}{A} \tag{25}$$

where q is the geothermal potential, A is the area of the cavern surface which is geothermally activated, $\dot{V}$ the volumetric flow rate, and T_{out} and T_{in} respectively the outlet and inlet temperature of the HCF fluid.

3. Results

3.1. Influence of design conditions on geothermal potential

The analysis is focused firstly on the geothermal potential for scenarios with varying airflow velocities v_a, representing different ventilation conditions, and heat release conditions of the data centre containers, q_{data}. In addition, characteristics of the geothermal activation such as inlet temperature T_{in} and flow velocity of the heat carrying fluid inside the pipes v_f are varied. Two settings are used for the inlet temperature of the HCF in the simulations. The first scenario uses an inlet temperature T_{in} of 3 ℃, a typical value in practice to represent extraction operations. In the second scenario an inlet temperature of 24 ℃, equal to the ground temperature is used. This way the proportion of the geothermal potential originating from the air domain in the cavern can better be assessed. The results of these analyses are presented in Fig. 3.

The results present a first overview of the sensitivity of the overall geothermal potential that can be extracted to the variability of the included parameters. Higher values of geothermal potential are found for higher heat release rates in the data centre cavern, for higher values of airflow velocities v_a and for higher fluid flow velocities of the HCF, v_f. The range of airflow velocities considered represents realistic airflow conditions in such a cavern to allow for suitable working conditions. Using an inlet temperature of the HCF fluid equal to the initial ground temperature results in a lower geothermal potential for the activated section, as only the aerothermal contribution is relevant.

The impact of the heat release q_{data} in the cavern on the geothermal potential is assessed. However, in practical applications, since a temperature limitation in the data centre would need to be satisfied, this heat release parameter cannot be considered as an independent engineering design variable and thus cannot be changed to enhance the performance of the geothermal system. This is different from the other two analysed parameters, the inlet temperature and flow velocity of the HCF.

3.2. Influence of geothermal activation on the temperature of the air domain

The impact of geothermal activation on the air temperature in the cavern is then assessed by comparing air temperature profiles with and without geothermal activation in the model. This comparison is shown for varying scenarios in ventilation conditions in Fig. 4, where for one vertical plane along the length of the cavern two-dimensional air temperature plots are created. The heat release from the data centre containers is scaled by the same percentage as the airflow velocity for preventing scenarios with unrealistically high air temperatures in the data centre cavern. Fig. 5 shows the temperature difference between the geothermally activated and non-activated solutions in both the air domain and the surrounding ground domain. In Fig. 6 the influence of geothermally activating one wider section or multiple sections in the cavern on the air temperature for the ventilation scenario used in Fig. 4B is illustrated. In this figure x_{GHE} represents the width of the geothermally activated section and L_{cavern} is the total cavern length.

The effect of the geothermal activation is shown in Figs. 4, 5 and 6, where a temperature reduction after the geothermally activated section following the direction of airflow in the centre is observed. The decrease in air temperature is observed in a certain region, which is dependent on conditions like the width of the geothermally activated part and the airflow conditions in the cavern. This zone of influence is longer with higher airflow velocities in the cavern. In other words, the length of the cavern where a cooling effect is obtained due to geothermal activation of one section is longer and the cooling is more distributed because of the higher airflow velocity. This cooling effect is not only obtained in the air domain of the underground data centre, but as can be seen in Fig. 5, this is also observed in the rock domain surrounding the caverns. At the location of the geothermally activated section, x = 150 m, a large cooling effect of the ground is introduced due to the circulation of the HCF at this position. At this position a large zone with a temperature change of more than $\Delta T = -2$ ℃ is obtained. At the other locations the cooling of the ground domain is in the range from −1 to 0 ℃, with more cooling in the air domain than the rock domain.

Fig. 6 highlights that increasing the width of the geothermally activated section in the model shows a higher reduction in the air temperature and likewise increasing the number of geothermally activated sections at different positions in the model also shows an increased impact on the temperature reduction in the air domain. The average temperature of the air domain in several models with an increasing number of activated sections in the cavern is calculated and is presented in Table 3.

3.3. Reduction in ventilation requirement

From the previous finding, optimization of the system by a reduction in mechanical ventilation requirement through geothermally activating the data centre is assessed. During normal operation the ventilation requirements are derived from a temperature limitation inside the

Table 2
Model parameters used in the thermal analyses.

	Parameter	Symbol	Value	Unit
Ground	Temperature	T_{ground}	24	°C
	Thermal conductivity	λ_{ground}	3.1	W/(m·°C)
	Density	ρ_{ground}	2160	kg/m^3
	Heat capacity	$c_{p_{ground}}$	926	J/(kg·°C)
Air	Airflow velocity	v_a	2*	m/s
	Inlet airflow temperature	$T_{a,in}$	24	°C
	Dynamic viscosity	μ	1.814E-5	Pa·s
	Thermal conductivity	λ_a	0.026	W/(m·°C)
	Density	ρ_a	1.204	kg/m^3
	Heat capacity	c_{p_a}	1005	J/(kg·°C)
	Wall roughness	k_s	0.3	mm
Shotcrete	Thickness	t_s	150	mm
	Thermal conductivity	λ_s	2.3	W/(m·°C)
	Density	ρ_s	2400	kg/m^3
	Heat capacity	c_{p_s}	843	J/(kg·°C)
Pipe	Internal diameter	d_{pipe}	20	mm
	Wall thickness	t_{pipe}	2	mm
	Thermal conductivity	λ_{pipe}	0.35	W/(m·°C)
HCF	Fluid		Water	–
	Flow velocity	v_f	1*	m/s
	Inlet temperature	T_{in}	3*	°C
	Thermal conductivity	λ_f	f(T) (a)	W/(m·°C)
	Density	ρ_f	f(T) (b)	kg/m^3
	Heat capacity	c_{p_f}	f(T) (c)	J/(kg·°C)
Data centre containers	Heat release	q_{data}	125*	W/m^2

* *Unless specified otherwise.*

(a) $\lambda_f(T) = -0.869083936 + 0.00894880345 \cdot T - 1.58366345E^{-5} \cdot T^2 + 7.97543259E^{-9} \cdot T^3$

(b) $\rho_f(T) = \begin{cases} -950.704055329848 + 18.9229382407066 \cdot T - 0.060367639882855 \cdot T^2 + 0.000063092789034 \cdot T^3, 0 < T < 20^{\circ}C \\ 432.257114008512 + 4.969288832655160 \cdot T - 0.013395065634452 \cdot T^2 + 0.000010335053319 \cdot T^3, 20 < T < 100^{\circ}C \end{cases}$

(c) $c_{p_f}(T) = 12010.1471 - 80.4072879 \cdot T + 0.309866854 \cdot T^2 - 5.38186884E^{-4} \cdot T^3 + 3.62536437E^{-7} \cdot T^4$

facility. Fig. 7 gives an overview of the complete system in the underground data centre cavern, where there are different influences on the air temperature and they all centre around respecting this temperature limitation in the air domain. The limitation originates from the need of providing acceptable work conditions in the data centre. Further requirements on ventilation results from the need for periodic air exchange, for maintaining an acceptable air quality, and in case of fire emergency. For air exchanges in working areas, an exchange time of 20 min for the 300 m long cavern would produce a minimum air velocity of 0.25 m/s, while for fire scenarios an air velocity of 1.0 to 1.5 m/s may be desirable to guide the smoke while maintaining stratification. Air quality control, beyond temperature control, is expected to be low for the largely emission-free installations in a data centre.

In this framework, the work domain of the data centre is defined as shown in blue in Fig. 8. It includes the air domains between the data centre containers and the cavern side walls, positioned after the geothermally activated section following the direction of airflow. Using a limitation of 32 ℃ of the average air temperature in this work domain then allows assessing the ventilation requirement needed for different scenarios of geothermal activation.

It is found that geothermally activating a section of the underground data centre can lead to a reduction in ventilation requirement (airflow velocity) for situations where this requirement is determined by a temperature limitation. Considering a wider section of geothermal activation in the cavern shows a larger reduction in the airflow velocity v_a, as shown in Fig. 9. For this evaluated scenario the required airflow velocity from the ventilation system could be reduced with 44 % by geothermally activating 15 sections, representing a width of 8.8 % of the total length of the cavern, before the work domain. This assessment is primarily conducted for the scenario depicted in Fig. 9, with a focus on these specific design variations. To further enhance the system's performance, a broader range of design parameters and variations can be explored.

3.4. Discussion

The ability of geothermal activation to reduce air temperature in the work domain within the alleys between the rows of containers is presented in the previous sections. However, some limitations and uncertainties in the study need to be discussed. No experimental validation of the case study result is possible at the moment as monitoring results in real conditions are not available at this stage.

Other uncertainty derives from the definition of the working area in this optimization study. In reality, ventilation requirements are strongly dependent on the distance from the heating container surface at which the temperature requirements need to be upheld. This factor is not accounted for in the simulations. Another factor that should be considered is that the analysis of optimization of ventilation requirements was done considering the average air temperature of the work domain. It is likely that the performed analysis overestimates the efficiency of the activation in terms of benefits of ventilation requirement reduction, because a reduction in longitudinal airflow leads to larger temperature variations in the air domain. This will decrease the average temperature quicker than the maximum temperature in the same volume.

Furthermore, it is important to realize that a decoupled modelling approach is used in this study, where a one-way coupling is used to assess the influence of geothermally activation on the air temperature. Using this one-way coupling results in a large reduction in computation time. However, it is important to look at the impact on the results that this simplification causes. Two main effects are not accounted for due to the one-way coupling; these are further described below.

- The data containers in the underground data centre release heat in the form of a heat flux in the numerical model. This causes an increase in the air temperature in the cavern, which in reality decreases the density of the air considering that the pressure conditions are not affected. With a lower air density, this warmer air is expected to rise

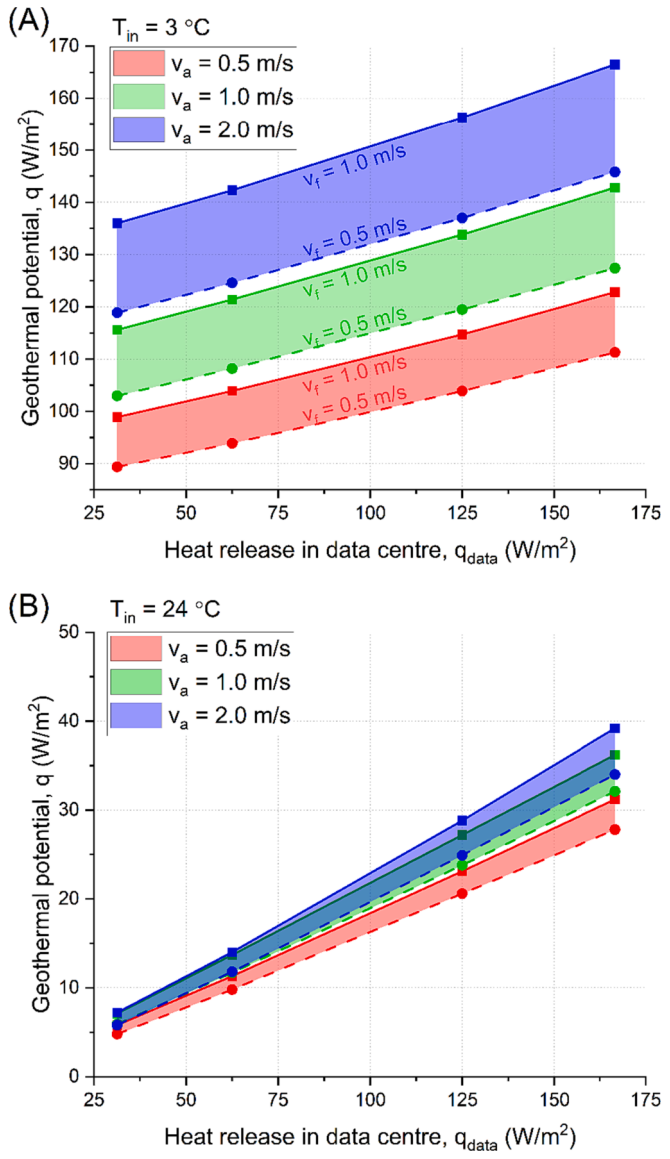

Fig. 3. Geothermal potential in an underground data centre cavern for varying airflow velocities, v_a, and HCF flow velocities, v_f, for (A) T_{in} = 3°C and (B) T_{in} = 24°C.

up in the cavern air domain. This effect is not accounted for due to the one-way coupling where the k-ω turbulent flow model is solved without considering these temperature variations. The air density change introduced due to the change of the average air temperature because of this component is approximately 0.039 kg/m^3, which represents a decrease of 3 % and is not significant.

- Geothermal activation of a section of the cavern introduces a local cooling effect. This causes a decrease in the temperature at some locations of the air domain, as shown in Fig. 5. This lower air temperature causes a higher air density and thus this is expected to introduce a sinking effect of the air that is cooled. Geothermal activation of the cavern is introduced in the floor and walls of the cavern, which means that the local zone where this cooling effect occurs is for a large part at the lower section of the air domain and thus the localised error is mainly expected along the activated walls of the air domain. To some extent the geothermal activation counteracts the decrease in air density following the heat generation in certain zones but amplifies the local differences of this parameter.

It can thus be stated that a potential for reducing the normal operation requirements of the cavern ventilation system is clearly recognizable from the results of this study, however a more precise quantification of this effect would be required for practical application. Therefore, it is important that these numerically obtained results are verified with experimental studies in the future.

4. Broader perspectives

4.1. Design optimization framework

A correlation is developed to make estimates of the geothermal potential more readily available for varying boundary conditions. The approach is based on Nusselt correlations, which are widely used to estimate convective heat transfer coefficients based on dimensionless analysis of empiric data. Nusselt correlations generally have the form of the Nusselt number being dependent on the Reynolds and the Prandtl number, where the Nusselt number, Reynolds number and Prandtl number are defined as

$$\mathrm{Nu}_L = \frac{hL}{\lambda_a} \tag{25}$$

$$\mathrm{Re}_L = \frac{v_a L}{\nu} \tag{26}$$

$$\mathrm{Pr} = \frac{\nu}{\alpha} \tag{27}$$

with L being a characteristic length of the geometry in question, h the convective heat transfer coefficient, λ_a the thermal conductivity, ν the kinematic viscosity and α the thermal diffusivity.

With the geothermal activation being situated 150 m along the cavern (for most simulations), airflow is expected to be fully developed ($x \gg 10{*}d_h$) and a correlation based on the hydraulic diameter ($L = d_h$) is used. To determine a viable correlation, fit for estimating the geothermal potential when activating the data centre cavern, a form similar to the equations by Dittus-Boelter or Chilton-Colburn (Laloui & Rotta Loria, 2019)

$$\mathrm{Nu} = \mathrm{f}(Re, Pr) = C{\cdot}Re^x{\cdot}Pr^y \tag{28}$$

is used. This correlation is primarily aimed at determining the heat transfer coefficient in turbulent pipe flows. There are significant differences, which make the Dittus-Boelter equation not directly applicable to this scenario, such as the cross-section geometry and wall roughness, or the spatial variation of the heat transfer process (both along the perimeter as well as in flow direction). The parameters C, x and y are not retained but the general shape of the correlation is. As the Prandtl number does not vary significantly across the flow field, its exponent is considered constant at y = 0.33, as it is found in Chilton-Colburn. Dittus-Boelter suggests a value of 0.4 when the fluid is heated and 0.3 when the fluid is being cooled, however as in this case study both processes appear in the same cross-section (cooling wall and heating container surface) an approach with a singular value is preferred.

For the identification of C and x, the Reynolds number is evaluated from the operating conditions while the Nusselt-number is extracted from the simulation results. As a result, values from C and x are determined based on simulations performed with several model variations. Model variations included scaling of the cross section, having a square cavern and different numbers of geothermally activated sections and data centre containers. The results in terms of the relation between Nusselt and Reynolds number of the airflow are illustrated in Fig. 10 and the obtained Nusselt correlation is

$$\mathrm{Nu} = \mathrm{f}(Re, Pr) = 7.192{\cdot}Re^{0.385}{\cdot}Pr^{0.33} \tag{29}$$

Using this correlation, the Nusselt number can be predicted based on the Reynolds number of the airflow and can then be used to have a first estimate of the geothermal potential for underground data centres with

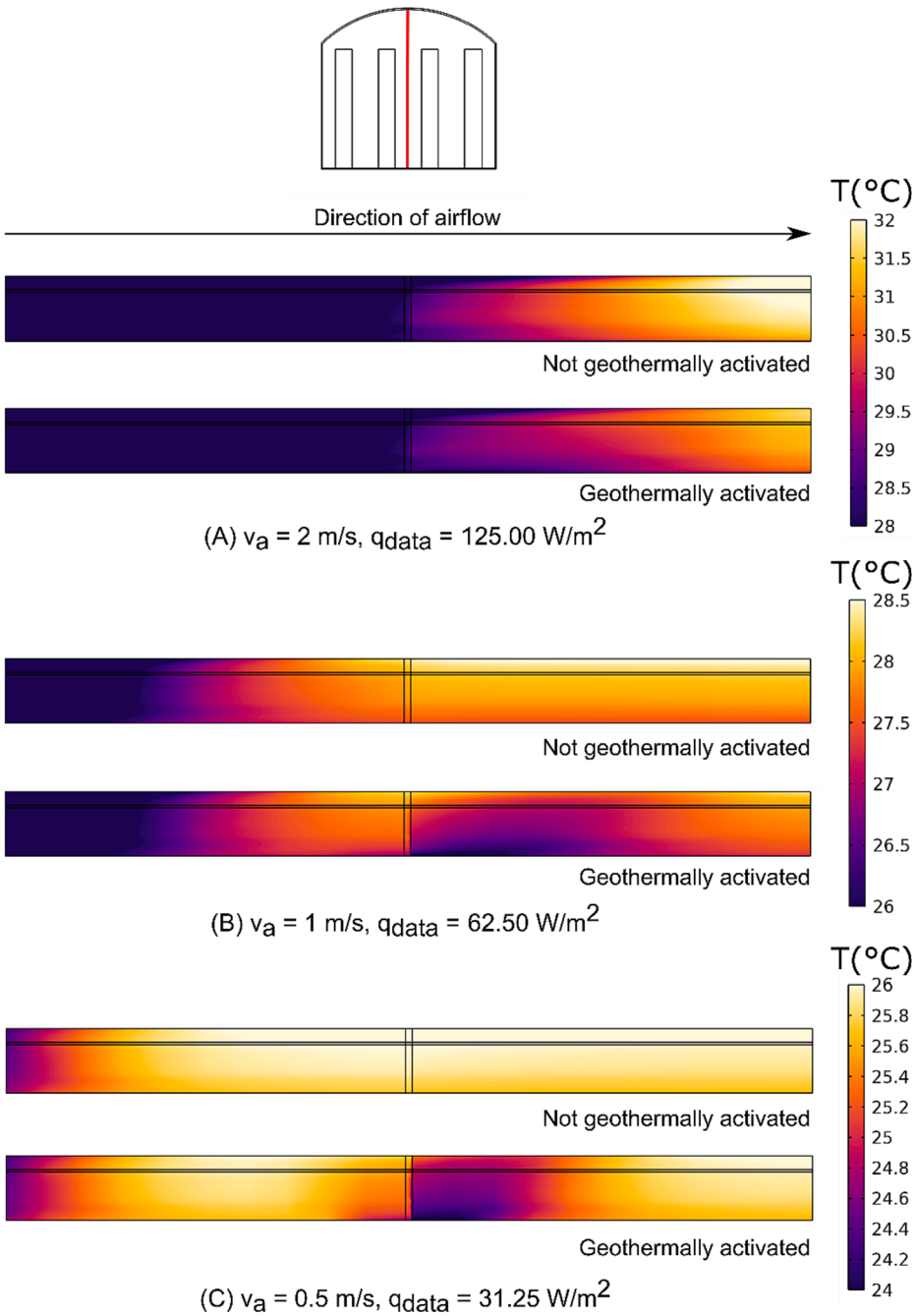

Fig. 4. 2D plots of air temperature in the underground data centre cavern for different scenarios of airflow velocity, v_a, and heat release from the data containers, q_{data}, for the full length of the cavern along its symmetry plane as indicated with the red line in the cross section. (For interpretation of the references to colour in this figure legend, the reader is referred to the web version of this article.)

similar settings.

4.2. Economic considerations

The impact of the findings in this study is explored by looking at their benefits in costs reduction and impact on greenhouse gas emissions for the underground data centre. The study with 8.8 % of the cavern length geothermally activated for evaluating the reduction in ventilation requirements as presented in Fig. 9 is taken as a reference case for these analyses.

The optimized geothermally activated cavern is compared in terms of costs to the normal cavern without geothermal activation. Both capital expenditures (CAPEX) and operational expenditures (OPEX) are evaluated. The scope of this analysis is presented in Table 4.

The capital investment in the construction of the underground data centre cavern is not included in the evaluation since this cost is independent of the analysis focussing on the impact of the geothermal activation on the financial overview. Similarly, the capital investment for the ventilation system is not included. Fan size and other characteristic parameters of the ventilation system are most likely determined by emergency situations. Therefore, the capital investment of the ventilation is considered to be the same for both situations and not included in this comparison.

The analysis follows the methodology developed for the study on the feasibility and energy performance of an energy segmental lining for a subway tunnel by Cousin et al. (2019). The following components are

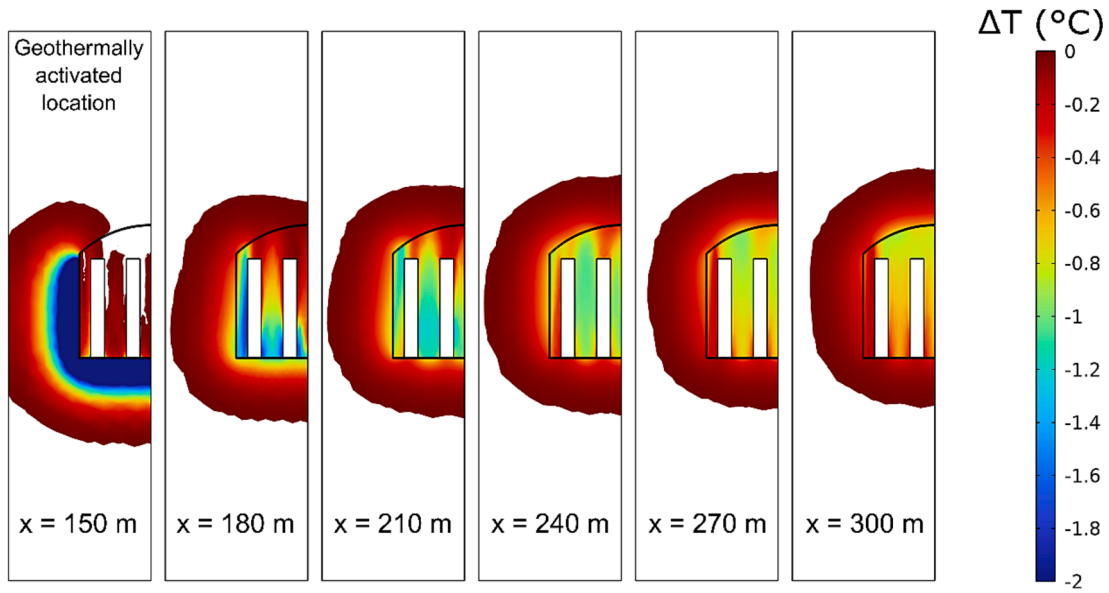

Fig. 5. Cross sections at different locations of the cavern showing the temperature difference between the not geothermally activated and geothermally activated scenarios. The results refer to scenario with an airflow velocity, v_a of 2 m/s and a heat release, q_{data} of 125 W/m^2.

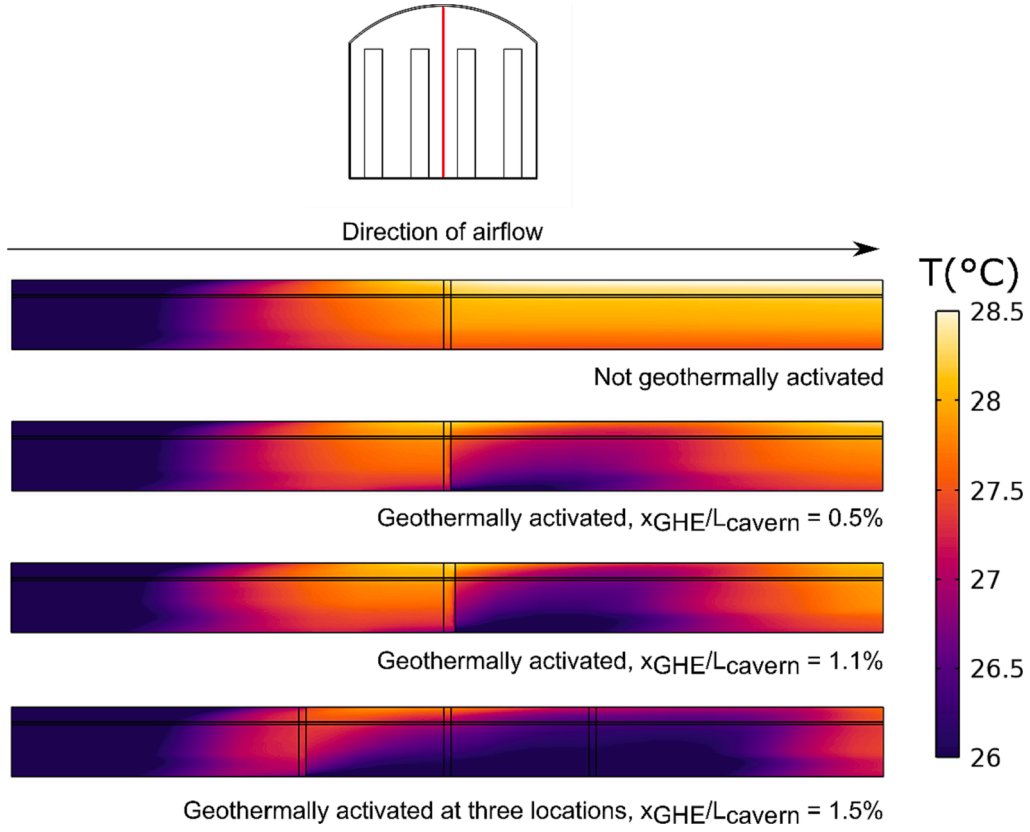

Fig. 6. 2D plots of air temperature in the underground data centre cavern for different scenarios of geothermal activation for the full length of the cavern along its symmetry plane as indicated with the red line in the cross section. The results refer to a scenario with an airflow velocity, v_a of 1 m/s and a heat release q_{data} of 62.5 W/m^2. (For interpretation of the references to colour in this figure legend, the reader is referred to the web version of this article.)

Table 3
Comparison of average temperature of the whole air domain for several analysed models with increasing number of geothermally activated sections.

Model	Average temperature air domain, T_{air} (°C)	Average reduction in temperature air domain (°C)
No geothermal activation	29.75	0.00
1 geothermally activated section	29.56	0.19
3 geothermally activated sections at 50 m intervals	28.87	0.88
15 activated sections at 20 m intervals	26.64	3.11

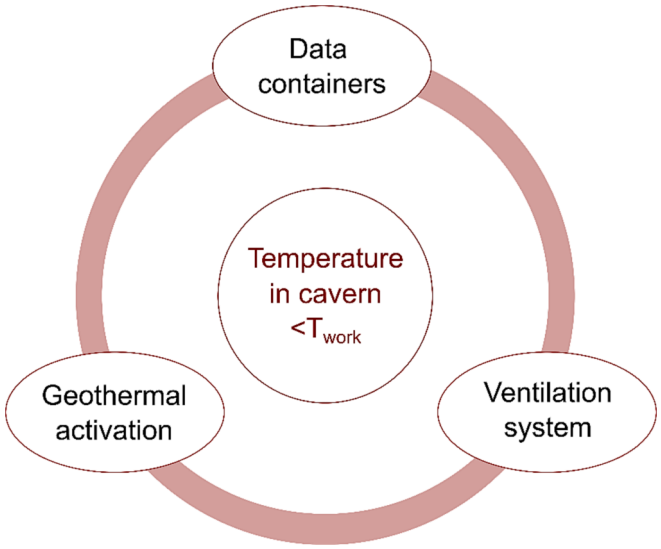

Fig. 7. Overview of key aspects for the temperature analysis of an underground data centre system with geothermal activation.

included in the calculation of capital expenses of the geothermal activation: piping (incl. mesh, tools and fittings), the circulation pump, the distribution network, labour effort and the heat pumps needed. As operating costs of this system, compressor pumping, circulation pumping and maintenance are included in the analysis.

The operational expenses of the ventilation system are calculated for the normal cavern situation and the optimized scenario where a reduced airflow velocity is needed to satisfy the air temperature limitation condition, as previously obtained. The running costs of a ventilation system are assumed to be proportional to the power consumption of its fans. This power consumption, P_{fan}, is computed based on

$$P_{\text{fan}} = \frac{1}{\eta_{\text{fan}}} \cdot \Delta p \cdot \dot{V}_a \tag{30}$$

where η_{fan} is the efficiency of the fan. This expression shows that the power consumption of the fans is proportional to the product of Δp and $\dot{V}_a$, which are the pressure losses and the airflow in the system. Pressure losses induced by airflow show a quadratic relationship, $\Delta p \sim \dot{V}_a^{\,2}$. This leads to a cubic scaling from airflow to power requirements within the same geometry, $P_{fan} \sim \dot{V}_a^{\,3}$. As a result, reducing the airflow requirements in normal operation is a very effective way of reducing the operation costs of the ventilation system. The reduction of required airflow velocity for the evaluated case study was approximately 44 %. This leads to the comparison of ventilation operational expenses presented in Fig. 11. It can be seen that a reduction of approximately 70 % of the yearly ventilation operation costs is achieved for the optimized scenario.

The profitability of the system is assessed through the calculation of the net present value (NPV) for both scenarios, which is defined as

$$NPV = -I_0 + \sum_{t=0}^{T_{service}} \frac{C_t}{(1+i)^t} \tag{31}$$

in which t is the time expressed in years, I_0 is the initial investment of the geothermal activation, $T_{service}$ is the service lifetime of the geothermal activation without additional investments taken as 25 years in this example, C_t is the yearly cash flow, made up from the yearly operational expenses and income generated from the operation of the thermal power plant and i is the sum of the inflation and interest rate taken as 3 % for this case. It is assumed that there is at least one year of time between the construction of the cavern and the start of operation of the data centre. No operational expenses are considered in this first year.

The generated income from the extracted thermal power is calculated based on a heat selling price (HSP) and assuming that all of the geothermally extracted heat is sold. A sensitivity analysis to the influence of the heat selling price is considered in the study, using a range from 75 EUR/MWh, which approximates the average heat selling price for a district heating network in a region in France in 2015 (AMORCE, 2016) to 120 EUR/MWh which was used in Cousin et al. (2019). The results are presented in Fig. 12Aand 12B.

A large variability results for the variation of the HSP, showing the importance of this parameter on the NPV over time. Initially the expenses are largest for the geothermally activated cases, due to the investment needed for the installation. After this initial investment however, the yearly net revenues for the geothermally activated cases become positive, due to the geothermally extracted heat that is sold. In the normal scenario, only the operational expenses of the ventilation system are accounted for which gives a negative yearly net revenue. When comparing the optimized scenario to the normal scenario without geothermal activation it is seen that a positive return on investment

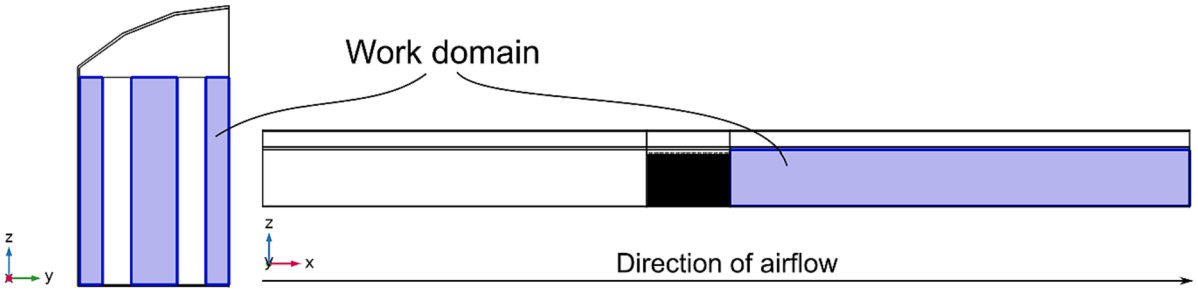

Fig. 8. Definition of the work domain where the temperature limitation is applied in the optimization evaluation.

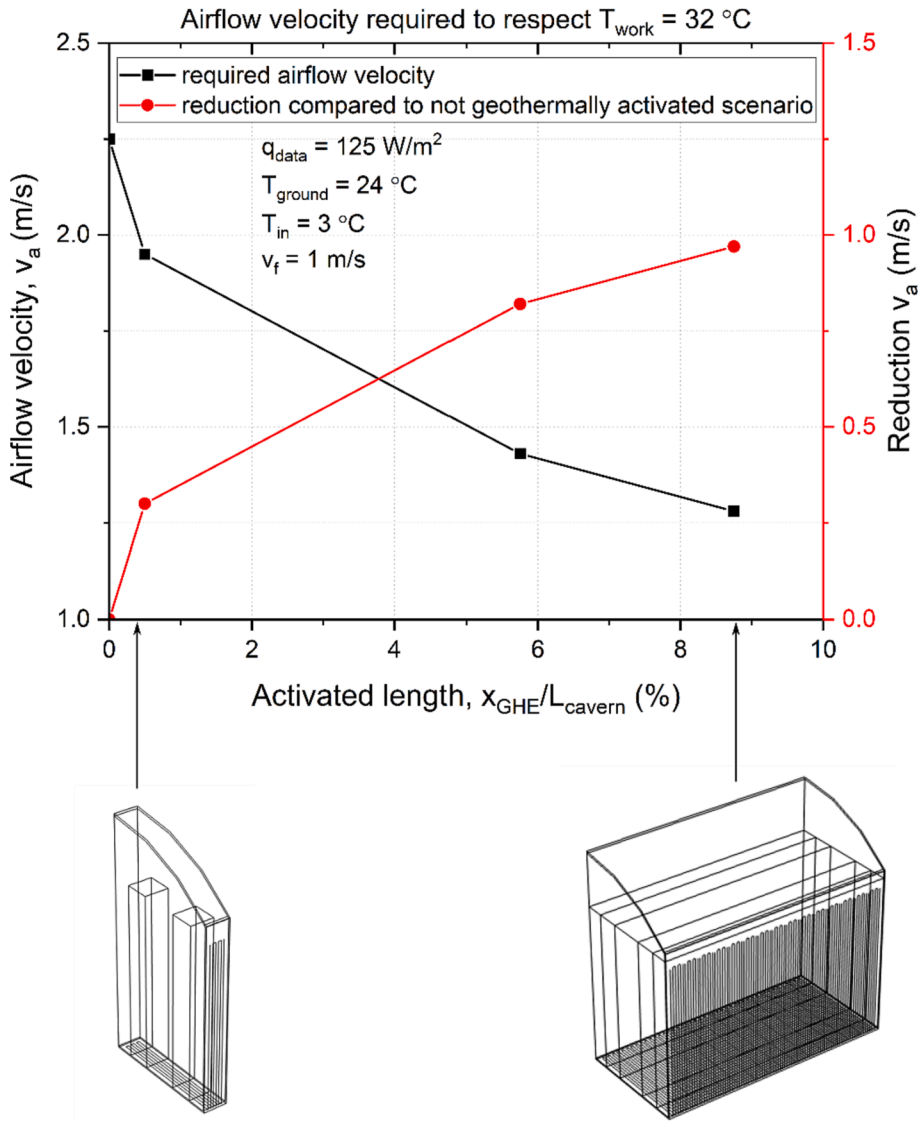

Fig. 9. Relation between airflow velocity, v_a needed to respect the average temperature limitation T_{work} in the defined work domain and the length of geothermal activation, x_{GHE}/L_{cavern} in the cavern.

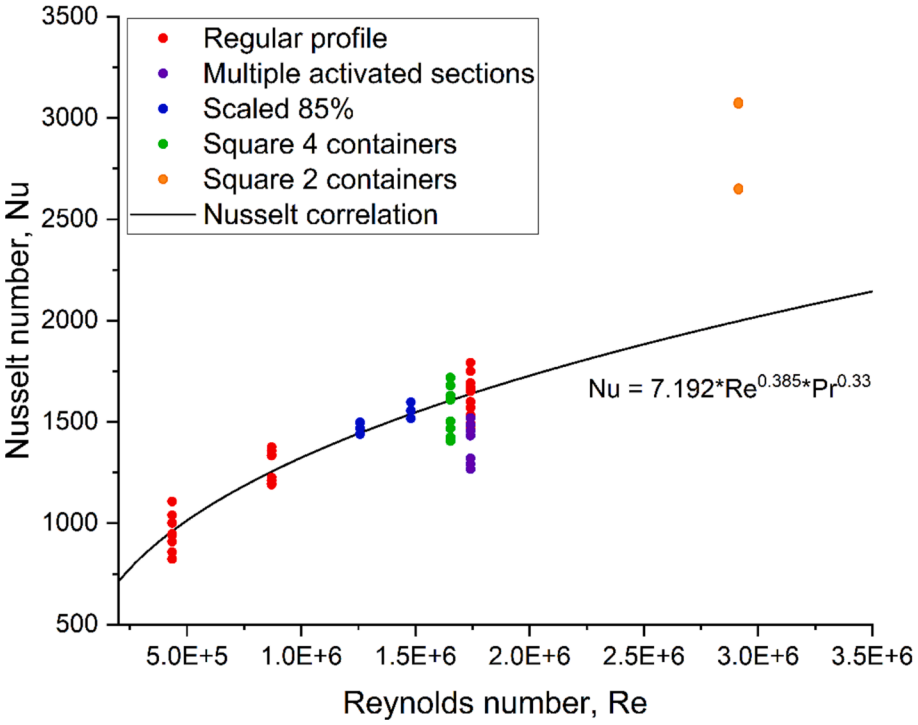

Fig. 10. Correlation between Nusselt and Reynolds number derived from model simulations.

Table 4
Overview of the scope of cost evaluation.

Optimized cavern	Normal cavern	Included or not
CAPEX underground cavern	CAPEX underground cavern	Not included
CAPEX geothermal activation	N/A	Included
CAPEX ventilation system	CAPEX ventilation system	Not included
OPEX geothermal activation	N/A	Included
OPEX ventilation system	OPEX ventilation system	Included
Heat sold (cash flow)	N/A	Included

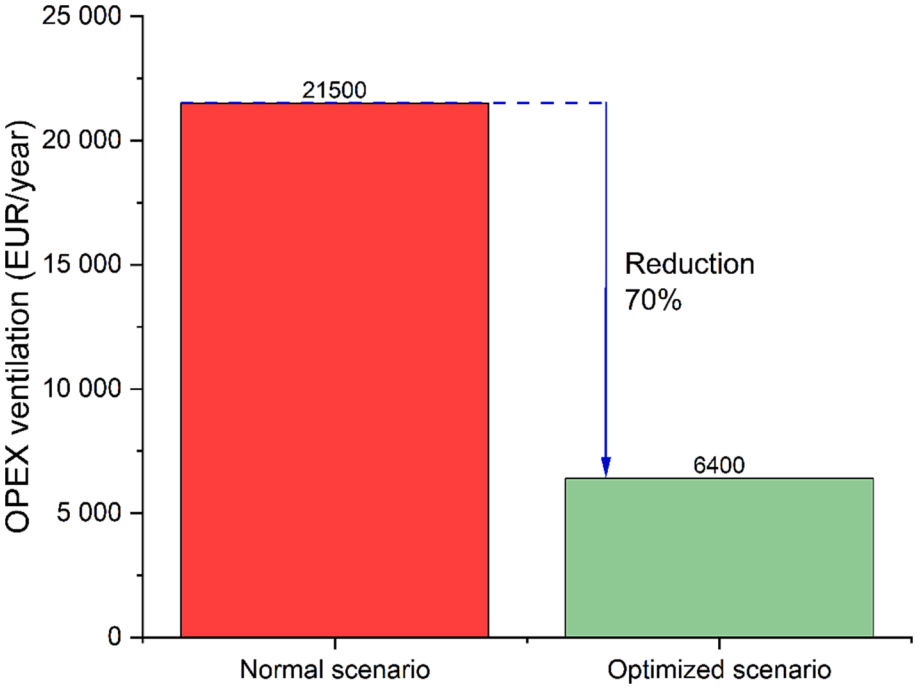

Fig. 11. Comparison of yearly operational expenses (OPEX) for the ventilation system.

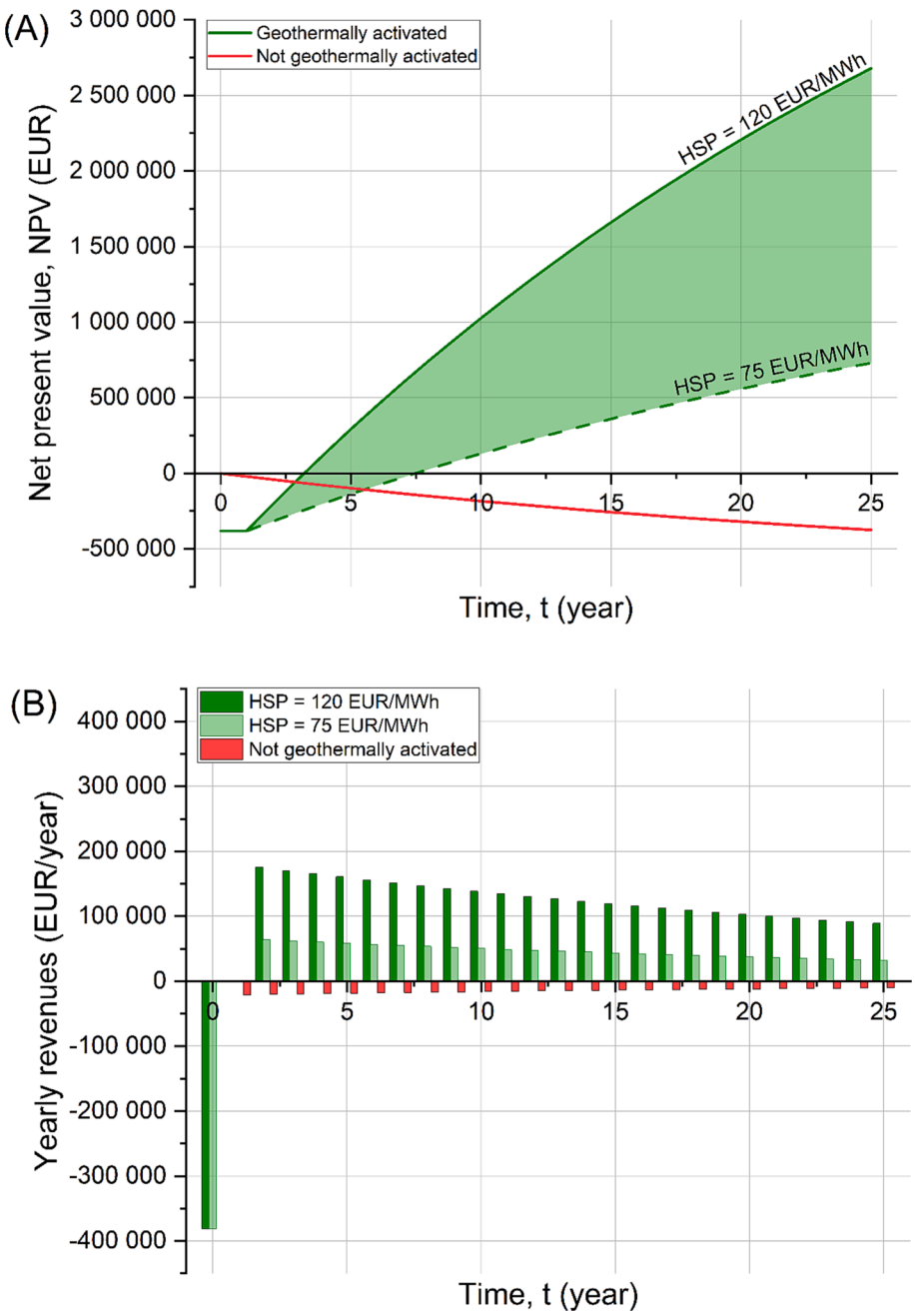

Fig. 12. Comparison of the (A) net present value and (B) yearly revenues over 25 years for two scenarios with geothermal activation and a range of the heat selling price, HSP between 75 and 120 EUR/MWh and the scenario without geothermal activation.

(ROI) can be expected between 3 and 7 years, depending on the value of the HSP used.

4.3. Environmental analysis

To further emphasize the environmental benefits of using energy geostructures, an evaluation of the greenhouse gas emissions due to the geothermal activation is made. The CO_2-equivalent (CO_2-eq) emissions resulting from electricity use by the geothermal system are compared to a reference scenario where the same amount of heating energy for buildings would have been provided by gas boilers. The CO_2-eq emissions for both scenarios are calculated using a carbon intensity parameter for a gas boiler and a carbon intensity value for a representative country of the underground data centre, as presented in Table 5. This leads to the comparison of the yearly CO_2-eq emissions as presented in Fig. 13. A reduction of 45 % in yearly CO_2-eq emissions is obtained, showing the large impact that geothermally activating underground data centres can have in terms of providing sustainable energy for

Table 5
Comparison of greenhouse gas emissions for energy production from geothermal activation or gas boilers.

	Energy from geothermal activation	Energy from gas boilers	
Electricity / energy requirement	785	2675.9	MWh
Carbon intensity factor	0.43 [1]	0.22 [2]	kg CO_2-eq/kWh
Total emissions per year	338	613	tCO_2-eq

[1] Electricity Maps (2022) [2]Cousin (2018).

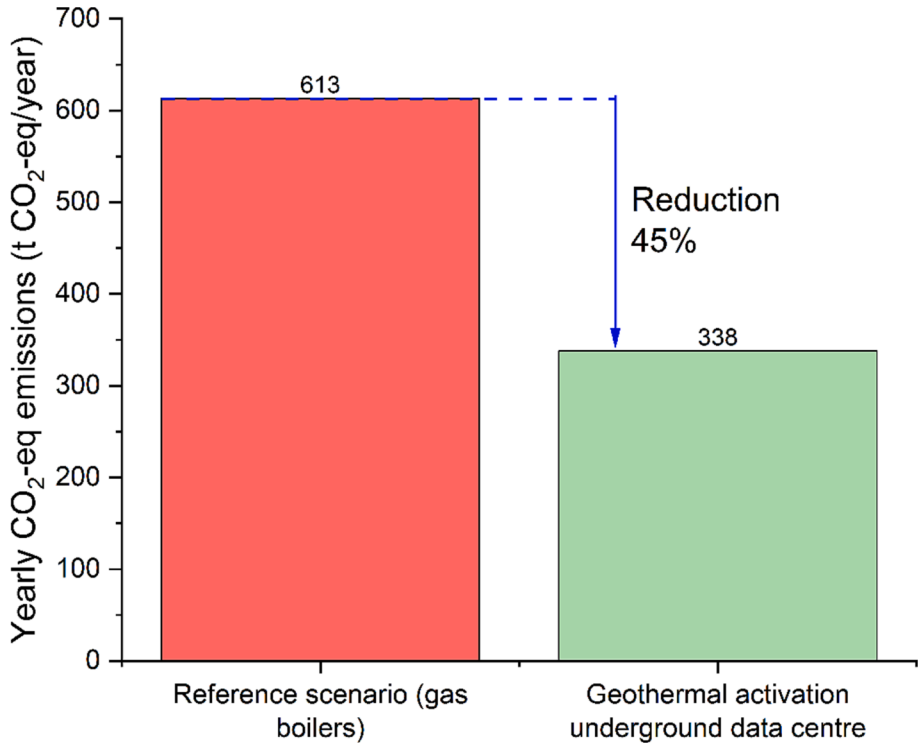

Fig. 13. Comparison of yearly CO_2-eq emissions for providing heating energy with gas boilers or through geothermal activation of the underground data centre.

heating purposes. Furthermore, the impact of emissions in the other life cycle phases was evaluated and it was found that these had little influence on the overall comparison.

5. Conclusions

This study explores for the first-time geothermal activation of underground data centres and the interface between ventilation and geothermal systems in this setting. Through numerical modelling the impact of geothermal activation on ventilation requirements in a cavern of a data centre is evaluated. The main conclusions of this work are:

- The sensitivity of the geothermal potential that can be extracted using one activated section in the underground data centre to several design parameters is explored. Higher airflow velocity, HCF velocity, or heat release in the underground data centre allow the extraction of a higher geothermal potential.
- Geothermal activation of a section in an underground data centre reduces the air temperature in a section after the position of the geothermal activation, following the direction of airflow. The location and length of this zone of influence depends on settings like the airflow velocity and the heat release of the data centre containers.
- This reduction in air temperature can be used to optimize the daily operation conditions of the ventilation system if these are determined by an air temperature limitation in a work domain. This is likely to be the case for an underground data centre. Quantifying the exact reduction in airflow velocity strongly depends on the case study characteristics and the definition of the temperature limitation.
- Geothermal activation of underground data centres has significant economic benefits. A return on investment of 3 to 7 years, using a heat selling price range of 75 to 120 EUR/MWh, is found when looking at the presented case study situation. A reduction of 70 % is obtained for specifically the OPEX of the ventilation system. These estimates assume that all the heat extracted through geothermal activation can be sold. In terms of environmental benefit, a reduction of 45 % in yearly CO_2-eq emissions is obtained if the geothermally extracted energy can be used for heating purposes instead of the same amount of energy from gas boilers. These results are obtained for a specific case study, a generalization cannot be made and the benefits need to be evaluated on a case by case basis.

CRediT authorship contribution statement

Sofie ten Bosch: Conceptualization, Methodology, Formal analysis, Investigation, Writing – original draft, Writing – review & editing, Visualization. **Elena Ravera:** Conceptualization, Methodology, Investigation, Writing – original draft, Writing – review & editing, Supervision. **Marco Tobler:** Conceptualization, Methodology, Formal analysis, Investigation, Writing – original draft, Writing – review & editing. **Marco Bettelini:** Conceptualization, Resources, Writing – review & editing, Supervision, Project administration. **Lyesse Laloui:** Conceptualization, Resources, Writing – review & editing, Supervision, Project administration, Funding acquisition.

Declaration of Competing Interest

The authors declare the following financial interests/personal relationships which may be considered as potential competing interests: the second author works at GEOEG – an engineering firm developing energy geostructures and the third and fourth authors work at Amberg Engineering – an engineering firm developing underground construction. The fifth author holds shares of GEOEG.

Data availability

Data will be made available on request.

Acknowledgements

This research was co-financed by Innosuisse, as Innovation project 58341.1 IP-EE.

References

AMORCE, 2016. Compétitivité des réseaux de chaleur en 2015—Comparatif des modes de chauffage et Prix de vente moyen de la chaleur (RCE26). AMORCE/ADEME. https://amorce.asso.fr/publications/competitivite-des-reseaux-de-chaleur-en-2015-comparatif-des-modes-de-chauffage-et-prix-de-vente-moyen-de-la-chaleur-rce26.

Bidarmaghz, A., Makasis, N., Fei, W., Narsilio, G.A., 2021. An efficient and sustainable approach for cooling underground substations. Tunn. Undergr. Space Technol. 113, 103986 https://doi.org/10.1016/j.tust.2021.103986.

Bidarmaghz, A., Narsilio, G.A., 2018. Heat exchange mechanisms in energy tunnel systems. Geomech. Energy Environ. 16, 83–95. https://doi.org/10.1016/j.gete.2018.07.004.

COMSOL, 2021a. COMSOL CFD Module User's guide (Version 6.0). COMSOL AB.

COMSOL, 2021b. *COMSOL Multiphysics Reference Manual* (Version 6.0). COMSOL AB.

Cousin, B., 2018. Feasibility and energy performance of an energy segmental lining for a subway tunnel. EPFL [MSc thesis].

Cousin, B., Rotta Loria, A.F., Bourget, A., Rognon, F., Laloui, L., 2019. Energy performance and economic feasibility of energy segmental linings for subway tunnels. Tunn. Undergr. Space Technol. 91, 102997 https://doi.org/10.1016/j.tust.2019.102997.

Dornberger, S.C., Rotta Loria, A.F., Zhang, M., Bu, L., Epard, J.-L., Turberg, P., 2022. Heat exchange potential of energy tunnels for different internal airflow characteristics. Geomech. Energy Environ. 30, 100229 https://doi.org/10.1016/j.gete.2020.100229.

Electricity Maps, 2022. Climate Impact by Area [Map]. https://app.electricitymaps.com/zone/HK?s=&lang=en.

IEA, 2017. Digitalization and Energy. IEA Publications.

Kuzmin, D., Mierka, O., Turek, S., 2007. On the implementation of the κ-ε turbulence model in incompressible flow solvers based on a finite element discretisation. Int. J. Comput. Sci. Math. 1 (2/3/4), 193. https://doi.org/10.1504/IJCSM.2007.016531.

Laloui, L., Rotta Loria, A.F., 2019. Analysis and Design of Energy Geostructures: Theoretical Essentials and Practical Application. Academic Press.

Makasis, N., Narsilio, G.A., Bidarmaghz, A., Johnston, I.W., Zhong, Y., 2020. The importance of boundary conditions on the modelling of energy retaining walls. Comput. Geotech. 120, 103399 https://doi.org/10.1016/j.compgeo.2019.103399.

Nikuradse, J., 1933. Strömungsgesetze in rauhen Rohren. In *Forschungsheft 361 (Beilage zu "Forschung auf dem Gebiet des Ingenieurwesens"*. VDI-Verlag GmbH. Ausgabe B Band 4 Juli/August 1933.

Peltier, M., Rotta Loria, A.F., Lepage, L., Garin, E., Laloui, L., 2019. Numerical investigation of the convection heat transfer driven by airflows in underground tunnels. Appl. Therm. Eng. 159, 113844 https://doi.org/10.1016/j.applthermaleng.2019.113844.

Rotta Loria, A.F., 2020. Energy geostructures: Theory and application. E3S Web Conf. 205, 01004. https://doi.org/10.1051/e3sconf/202020501004.

Wilcox, D.C., 2008. Formulation of the k-w Turbulence Model Revisited. AIAA J. 46 (11), 2823–2838. https://doi.org/10.2514/1.36541.

Wilcox, D.C., 1991. A half century historical review of the k-omega model. In: 29th Aerospace Sciences Meeting. 29th Aerospace Sciences Meeting, Reno, NV, U.S.A. https://doi.org/10.2514/6.1991-615.

Wojnarowicz, M., 2020. Thermo-hydro-mechanical behavior of energy tunnels. EPFL [MSc thesis].

Zannin, J., Ferrari, A., Kazerani, T., Koliji, A., Laloui, L., 2022. Experimental analysis of a thermoactive underground railway station. Geomech. Energy Environ. 29, 100275 https://doi.org/10.1016/j.gete.2021.100275.

Zhang, H., Shao, S., Xu, H., Zou, H., Tian, C., 2014. Free cooling of data centers: A review. Renew. Sustain. Energy Rev. 35, 171–182. https://doi.org/10.1016/j.rser.2014.04.017.